Facilitating Stochastic Resonance as a Pre-Emphasis Method for Neural Spike Detection

Cihan Berk Güngör[1,2], Hakan Töreyin[2]

[1] Department of Electrical and Computer Engineering, University of California – San Diego, San Diego, CA, USA
[2] Department of Electrical and Computer Engineering, San Diego State University, San Diego, CA, USA

E-mail: htoreyin@sdsu.edu

Received April 19, 2020
Accepted for publication xxxxxx
Published xxxxxx

Abstract

Objective: We aim to increase the number of neural spikes that can be detected in a single channel extracellular neural recording. *Approach:* We propose a pre-emphasis method facilitating stochastic resonance (SR), where we introduce the band-pass-filtered noisy extracellular recording to an overdamped Brownian particle in a monostable well. The x-position of the Brownian particle is the output of the proposed pre-emphasis method. Threshold is applied on the output for spike detection. To characterize the dynamics and the solution of the system, we use a synthetic dataset generated by adding Gaussian white noise at different intensities to an intracellular recording. Then, we evaluate and compare the spike detection performance of the proposed method on a public synthetic extracellular dataset. *Main results:* The proposed SR-based spike detection improves the signal-to-noise ratio (SNR) of the intracellular-based synthetic dataset as much as 7.35 dB and outperforms the state-of-the-art pre-emphasis methods in false positive and false negative rates in 15 of the 16 synthetic extracellular datasets, with 100% sensitivity and positive predictivity values in seven of the recordings. *Significance:* The method has the potential of significantly increasing the number of neurons that can be monitored from a single-channel extracellular recording.

Keywords: Extracellular spike detection, mono-stable well, stochastic resonance.

1. Extracellular neural monitoring and Stochastic Resonance

Information is communicated across the brain in the form of electrical action potentials, namely neural spikes, generated by neurons. By analyzing spike activity, it is possible to unveil the brain connectivity and how information is represented in the brain. In fact, spike analyses have led to remarkable advances such as understanding brain mechanisms of different actions [1-3] and the disruptions in the neural networks in case of neurological disorders [2-5]. The foremost step to spike analysis is extracellular neural monitoring, where electrodes placed in a neural tissue capture the electrical potential changes corresponding to activities of neurons nearby. The captured signal is first amplified and filtered to improve the signal-to-noise-ratio (SNR). The conditioned signal is then pre-emphasized on which thresholding is applied for spike detection. Spikes are sorted based on several features (e.g., principal components, wavelet coefficients) to specify activity of different neurons.

Researchers studying extracellular neural monitoring have proposed a wide range of pre-emphasis methods for accurate spike detection (e.g., simple band-pass filtering [6], superparamagnetic clustering [6], Teager energy operator

(TEO) [7], wavelet transform [6, 8], template matching [9], cepstrum of bispectrum [10], time-frequency analysis [11], morphological filtering [12]). In general, template-matching methods have demonstrated higher detection performances than other methods [13-15]. However, template matching does not achieve high detection rates for spikes of low-activity neurons [16], which is considered as one of the reasons limiting the typical number of neurons observed in a recording from a single electrode to ~5 to 10 [17-18].

With the ultimate goal of increasing the detectability of spikes, we investigate stochastic resonance (SR) as a pre-emphasis method. SR is a phenomenon observed in many nonlinear systems including biological neurons, whereby noise is counterintuitively used to reinforce weak signals ([19-22]). Initially introduced as a phenomenon to explain the observed periodicity in global climate dynamics [23], later, systems of a variety of fields ranging from biology to human perception have been shown to perform noise-enhanced detection of weak signals and thus facilitating communication and signal processing [24-26]. Previously, we demonstrated that, in a threshold-based spike detection system with band-pass filtering implemented as the pre-emphasis method, there is an optimum flicker noise intensity maximizing spike detection sensitivity [27]. In this study, we investigate a non-linear system facilitating the background noise to improve the SNR of an extracellular recording. Although several studies have demonstrated SR-enhanced detection of weak signals [28-31], SR is investigated in the context of SNR improvement for spike detection in extracellular recordings for the first time.

We begin with describing our method and perform a comparison against the widely-used pre-emphasizing methods on a synthetic dataset with varying background noise intensities in Section 2. In Section 3, we evaluate the performance of our approach on a public synthetic dataset [6] and compare our results against the state-of-the-art. We discuss our results in Section 4, which is followed by conclusion and potential future work in Section 5.

2. Datasets and methods

2.1 Stochastic Resonance

Stochastic resonance (SR) is a phenomenon, where noise is used to enhance weak signals. Typically, SR is used to detect weak periodic signals. A common mechanism to facilitate SR is observing the movement of a Brownian particle in a bistable well potential when the signal is applied on the particle as a velocity term [32]. In the steady state, the particle rests in one of the stable points. If a periodic signal is introduced to the system, the particle swings around the stability point. If the signal amplitude is small (subthreshold), it cannot cause the particle to cross the barrier between the two stable points. If some noise is added on the subthreshold signal, however, the noisy subthreshold signal can make the particle cross the barrier and reach the other stability point. If the added noise intensity is too large, the particle movement follows the noise. However, if the added noise is at an optimal level, the particle moves between the stable points at the same frequency as the subthreshold signal. In other words, there is an optimal noise level that causes the input signal to be amplified [32].

In this study, we investigate SR as a method to enhance neural signals. Then, a threshold is applied on the enhanced signal for spike detection. It should be noted that, for neural monitoring purposes, detected spikes should eventually be classified (spike sorting) to extract the activities of different neurons. Although the focus of our study is limited to spike detection, because performance of spike sorting algorithms depends on how well the waveform characteristics of neural spikes are preserved [6], we perform our SR analysis on a system that can preserve spike waveform characteristics. Therefore, rather than a bistable well, which can introduce non-linearities and discontinuities on the original spike waveforms, we perform our analysis using a monostable well. To understand how noise can enhance the signal, we can consider a hypothetical noise-free recording. In this case, the particle would move towards the walls of the well during spike events only. In an actual recording, where the signal has noise on it, the noise could cause the particle to make larger movements during the spike events, thereby amplifying the spike amplitudes. Like the bistable well case, the noise intensity should be at an optimal level. If the noise intensity is too small, it will not have much effect. If it is too large, the signal will be swamped inside the noise. Notably, noise-only portions of an actual recording would also cause the particle to move around the stability point. To limit those movements and improve the SNR further, we consider an overdamped system.

2.2 Datasets

We perform our analyses on two types of synthetic datasets (Figure 1). The synthetic-dataset-1 (SD1) is generated using an intracellular recording, *d11222*, from the hippocampus region CA1 of rats from the Collaborative Research in Computational Neuroscience (CRCNS) database [33]. We control the noise level by addition of zero mean gaussian white noise at different intensities. The dataset is 750 s long, sampled at 20 kHz, and consists of 628 spikes. We use SD1 to describe and investigate our pre-emphasis method and perform comparisons with three widely-used pre-emphasis methods; namely band-pass filtering, TEO, and wavelet transform. The synthetic-dataset-2 (SD2) is a public synthetic extracellular dataset [6]; which consists of 16 recordings grouped under four categories, Easy1, Easy2, Difficult1, and Difficult2. Each recording is 60 s long, sampled at 24 kHz, and consists of simulated spikes from three neurons. These synthetic recordings consist of spikes with waveform shapes

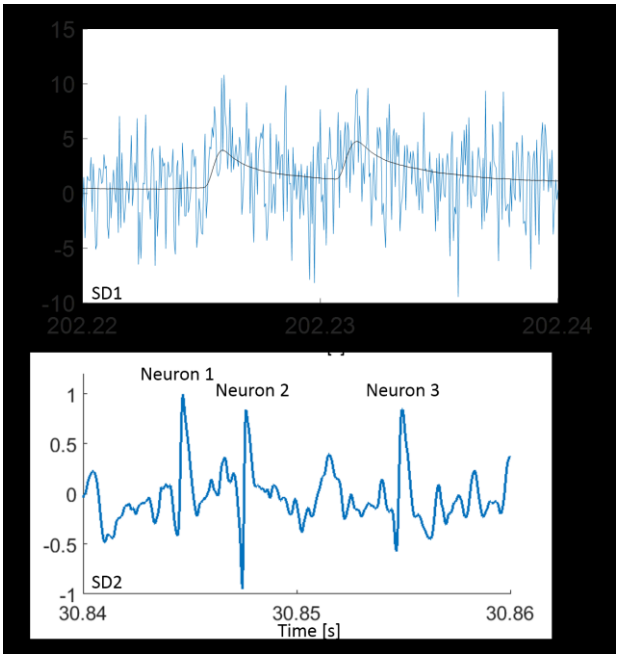

Figure 1. Close-up view to the spikes in the synthetic datasets used in the study. Top: Noise added on an intracellular recording. Bottom: Synthetic extracellular dataset in [6].

obtained from a database of ~600 spike shapes obtained from actual recordings in the neocortex and basal ganglia. The dataset mimics the background noise by including the small amplitude spikes from hypothetical distant neurons. The datasets contain spike trains with randomly-generated event times from three distinct neurons, each having an average firing rate of 20 Hz. The spike trains and noise are combined to generate the synthetic recordings. The noise levels correspond to the noise standard deviations normalized by the spike amplitudes.

In the literature, SD2 is widely used as a benchmarking dataset for evaluation of spike detection algorithms [12, 14, 15, 34-36]. Therefore, we use this dataset to validate the performance of our method on a realistic extracellular recording as well as do a direct comparison against the state-of-the-art spike-detection methods reported.

2.3 SR-based pre-emphasis

Our pre-emphasis method involves monitoring the movement of an overdamped Brownian particle in a nonlinear system, which is governed by the special form of the Langevin equation with neglected inertia term as [37]:

$$\frac{dx(t)}{dt} = -\frac{dU_0(x,t)}{dx} + s_n(t), \qquad (1)$$

where $x(t)$ is the x-position of the particle, $U_0(x,t)$ is a potential well that the particle interacts with; and $s_n(t) = s(t) + n(t)$ is a noisy signal with $s(t)$ and $n(t)$ being the signal and noise, respectively. A closer look into (1) reveals

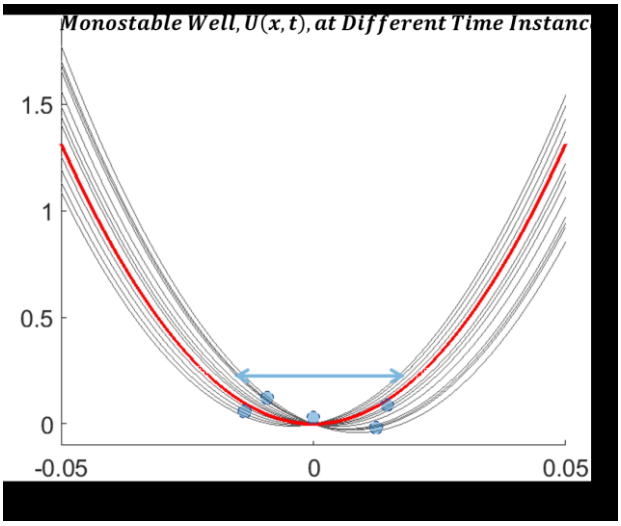

Figure 2. The proposed SR-based pre-emphasis method is based on the interaction of a Brownian particle in an overdamped monostable well. The original well, $U_0(x)$, drawn in red, has a stable point at x=0. Based on equation (3) in the text, the shape of the potential is changed depending on the band-pass filtered input signal, $s_{n,F}(t)$. The resultant potential wells corresponding to different time instances are drawn in black. The movement of the particle is also illustrated. For numerical solution of the particle movement, refer to equations (5)-through-(7) in the text. The system output is the x-position of the particle.

that, in this system, the velocity of the particle, $\frac{dx(t)}{dt}$, is controlled by two terms on the right-hand side of the equation. The first term, which has negative sign, represents the contribution of the potential well on the particle velocity. Essentially, the particle tends to move towards the stable point, which is the opposite direction to the sign of the well slope. The second term represents the contribution of the system input on the particle velocity. In our case, we introduce a band-pass filtered (BPF) version of the input signal, $s_n(t)$, to the particle. We use a Kaiser window, finite impulse response (FIR) filter with cut-offs 300 Hz – 6 kHz. The BPF output signal is $s_{n,F}(t)$.

To graphically understand the movement of the Brownian particle, we modify equation (1) such that both terms are incorporated inside a new time-dependent potential well, $U(x,t)$ [30]:

$$\frac{dx(t)}{dt} = -\frac{dU(x,t)}{dx}, \qquad (2)$$

where

$$U(x,t) = U_0(x,t) - x \cdot s_{n,F}(t). \qquad (3)$$

Based on (3), the monostable well, which the particle interacts with, has both temporal and spatial characteristics that collectively impact the movement of the particle. From (2), at a given time instant, the particle tends to move towards the stable point of $U(x,t)$ at a velocity equal to the amplitude of the slope of the well calculated at where the particle is

located. The output of the system is the x-position of the particle.

The last step before illustrating the particle movement in the well is defining the well potential. As previously mentioned in Section 2.1, for neural spike pre-emphasis application, we investigate a monostable well potential given as:

$$U_0(x) = ax^2/2 + bx^4/4. \quad a, b > 0 \qquad (4)$$

After replacing the monostable well expression in (4) inside (3), we illustrate the variation of $U(x,t)$ for a short-period, T, (T<1 ms) of an exemplary $s_{n,F}$ in Figure 2. The potential well drawn in red represents $U_0(x)$. The potential wells drawn in black represent $U(x,t)$ for different $t \in (0,T)$. To find the movement of the Brownian particle, we first combine the equations (2)-(4), leading to:

$$\frac{dx(t)}{dt} = -[ax(t) + bx^3(t)] + s_{n,F}(t). \qquad (5)$$

A flowchart representing the equation (5) is presented in Figure 3. In the digital domain, solution of (5), an ordinary differential equation, can be approximated by an iterative numerical method, namely the fourth-order Runge-Kutta (RK) method, described by [37]:

$$x[n+1] = x[n] + (k_1 + 2k_2 + 2k_3 + k_4)/6, \qquad (6)$$

where $x[n]$ is the nth sample of $x(t)$ and k_1 through k_4 are given as:

$$\begin{aligned} k_1 &= h\left[-ax[n] - bx^3[n] + s_n[n]\right] \\ k_2 &= h\left[-a\left(x[n] + \frac{k_1}{2}\right) - b\left(x[n] + \frac{k_1}{2}\right)^3 + s_n[n+1]\right] \\ k_3 &= h\left[-a\left(x[n] + \frac{k_2}{2}\right) - b\left(x[n] + \frac{k_2}{2}\right)^3 + s_n[n+1]\right] \\ k_4 &= h\left[-a(x[n] + k_3) - b(x[n] + k_3)^3 + s_n[n+2]\right]. \end{aligned} \qquad (7)$$

In (7), h is the interval size of the approximation; and $s_n[n]$, $s_n[n+1]$, and $s_n[n+2]$ are respectively the nth, n+1st, and n+2nd samples of $s_n(t)$. A graphical representation and a description of how RK method approximates the movement of the particle is provided in Figure 4 and its caption.

The change in the potential well and the response of the system at different time instances for non-spike and spike events are shown in Figure 5. The over-damped system cannot respond sufficiently fast to the rapid and arbitrary changes during non-spike regions; thereby causing the particle to remain in the proximity of the stable equilibrium point, $x = 0$ (Figure 5(c) - Left) A noisy spike on the other hand causes a persistent change in the well potential for a period that is sufficiently long to move the particle outside the equilibrium point (Figure 5(c) - Right).

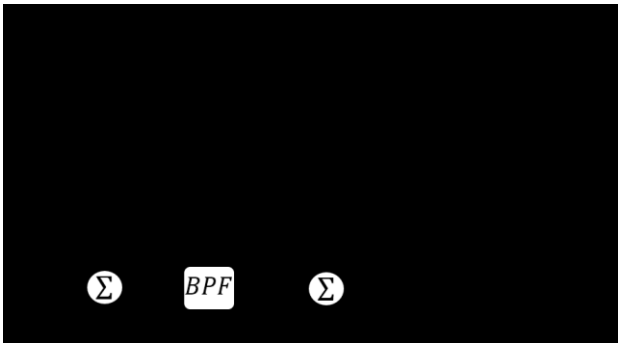

Figure 3. A flowchart of the differential equation, which is given in equation (5) in the text, solved to find the x-position of the Brownian particle in an overdamped monostable well. The differential equation is solved using the fourth-order Runge Kutta method described using equations (6)-(7) in the text.

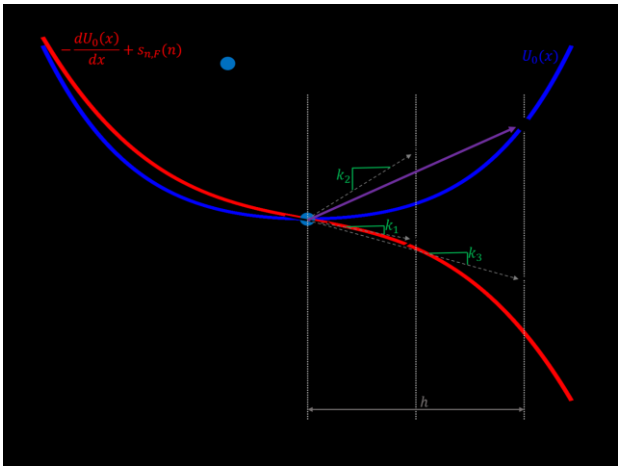

Figure 4. A graphical illustration of the Runge-Kutta (RK) method. The sum of the negative derivative of the well potential and the noisy input signal are evaluated at, *x[n]*, the original position of the particle at the nth data point to obtain a slope parameter k_1. Then, a new slope, k_2, is calculated using the sum evaluated at a new position informed by both the original particle position and the previous slope, k_1. The process is repeated to find two additional slopes, k_3 and k_4,. The *x[n]* and all calculated slopes are linearly combined to find *x[n+1]*.

In equations (3)-(5), proper selection of positive-valued $a, b,$ and h is critical to achieve high SNR at the output. In the literature, several SNR definitions are made in the context of spike detection [7, 8, 39-42]. We calculate the SNR as the ratio of the peak-to-peak amplitude (A_{pp}) of the minimum-amplitude spike in the dataset to the peak-to-peak amplitude of a noise-only portion of the recording:

$$SNR = 20log\left(\frac{App\ of\ spike\ with\ minimum\ amplitude}{App\ of\ a\ noise\ segment}\right). \qquad (6)$$

For noise A_{pp} calculation, 60 s and 2 s of total noise-only segment durations are used in SD1 and SD2, respectively.

We perform parametric search for the optimum values of *a, b,* and *h* maximizing the SNR. Variation of SNR for SD1 with

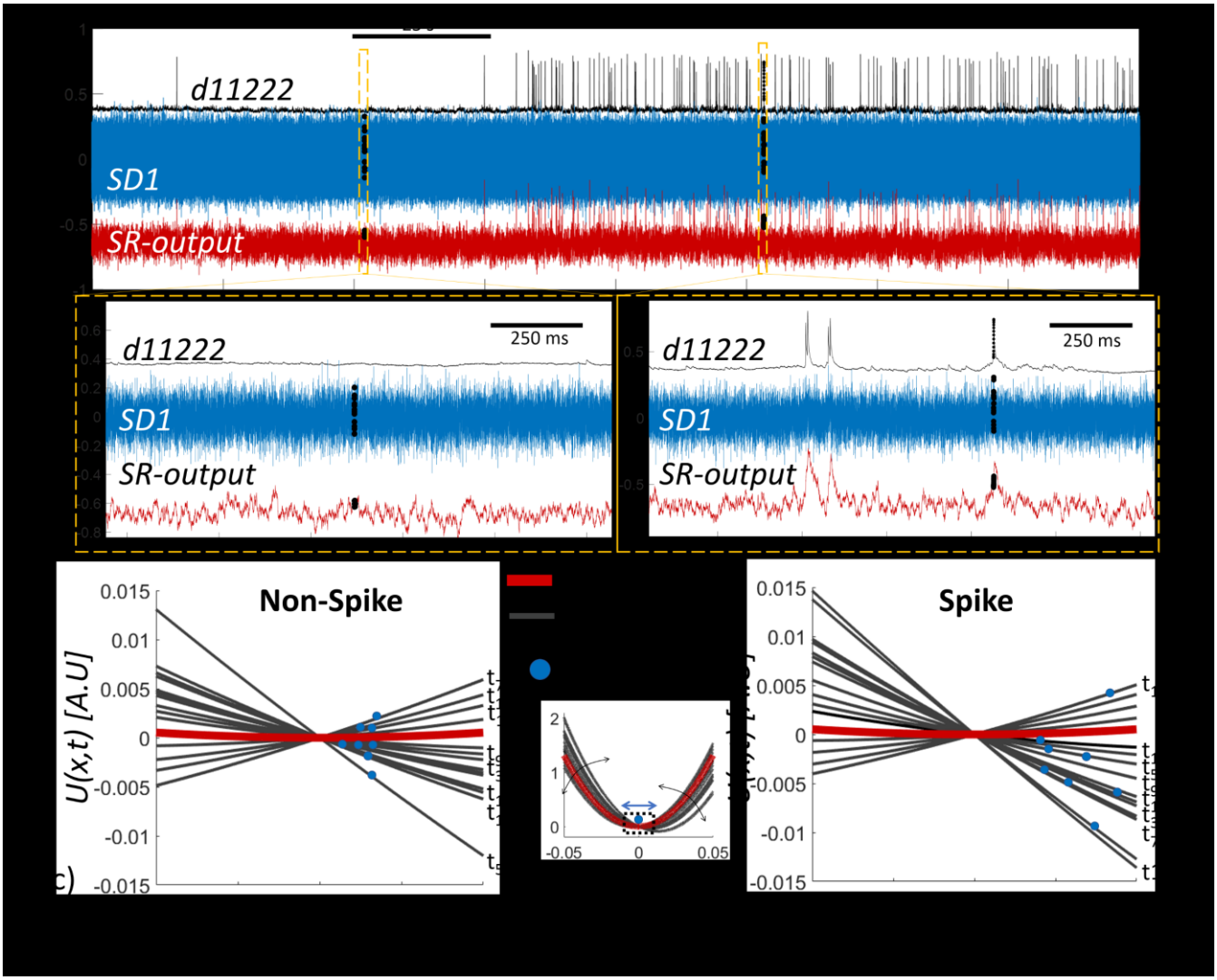

Figure 5. The response of the SR-based pre-emphasis method to non-spike (noise) and spike segments in SD1 with a noise-level of 10. (a) 200 s portion of SD1 and the SR-output. The intracellular recording *d11222* is shown to indicate the spike locations. Amplitudes of all waveforms are normalized for visualization purposes. The two highlighted segments show non-spike and spike cases. (b) The close-up view of the two highlighted segments in (a). The black dots represent the data points at which the well and the Brownian particle movements are illustrated in (c). Fifteen data points, t_1 through t_{15}, per case are used to show the changes in the well-shape for non-spike and spike cases. The data points for the spike event are selected as the time instances over which the spike in *d11222* is rising. (c) The well shape and the particle movement are shown (center). The red-line represents the original well shape, *U(x)*, with zero input. The black lines represent the changes in the well-shape. The movement of the particle is demonstrated on half of the data points. The dashed rectangle represents the close-up views of the changes for the non-spike (left) and spike (right) cases.

a noise level of 10 is presented in Figure 6. The output SNR is correlated more strongly to a than b for a given input noise level. This result is explained by the stronger dependence of U_0 to a than b values in (3) for x between -0.001 and 0.001, the dynamic range of the x-position of the particle moves for different datasets [Figure 6(a) inset]. Our parametric search has led to different optimum values for the a and h parameters for a range of background noise levels between 1 and 50. The corresponding input SNR, SNR_{in}, ranges between -1.16 dB and +0.3 dB. The corresponding output SNR, SNR_{out}, ranges between -1.2 dB to +7.65 dB (Table 1).

The dc level of the input signal impacts the stability point of the dynamic system. An input signal with zero mean, which indicates that the average added velocity of the particle is also zero, causes the particle to move around $x_0=0$. However, a positive (negative) dc level shifts the stability point to $x_0>0$ ($x_0<0$). The outputs of the system corresponding to SD1 with a noise level of 10 for three dc levels of [-20, 0, +20] are shown in Figure 7.

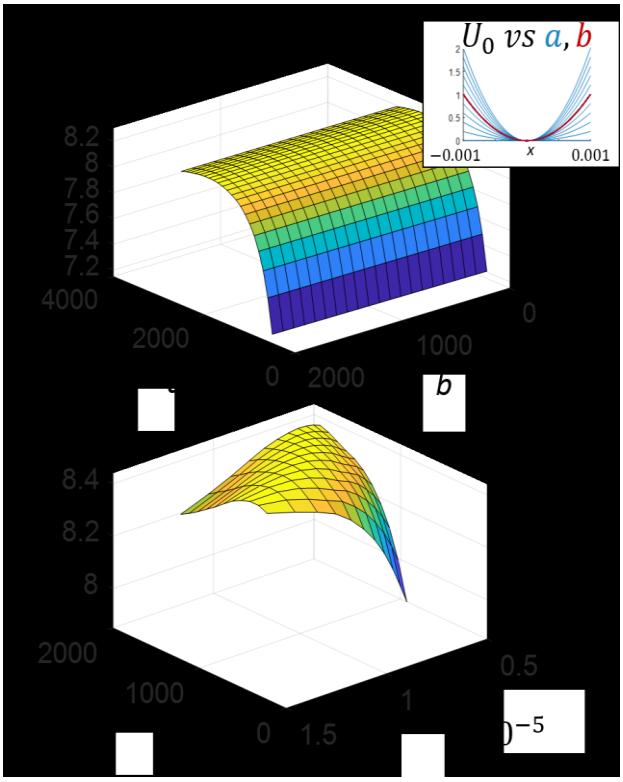

Figure 6. Parametric search to optimize *a*, *b*, and *h*. that would maximize the SNR. The results are given for SD1 with noise level: 10 (a) The parameter *b* has a weak control over the well potential, U_0 (Inset). Therefore, SNR is primarily dependent on the parameter *a*. (b) The SNR is strongly dependent on the well parameter *a* and the step-size parameter, *h*, of the Runge-Kutta approximation method.

Table 1. Optimum well and solver parameters for different background noise levels

Added Noise Level	SNR_{in} (dB)	*a*	*h*	SNR_{out} (dB)
1	0.3	960	1.47 x 10^{-5}	7.65
2	-0.71	970	1.09 x 10^{-5}	5.34
3	-0.81	1050	9.3 x 10^{-6}	3.98
4	-0.86	1050	1 x 10^{-5}	3.26
5	-0.96	1020	8.7 x 10^{-6}	2.93
6	-1.03	1050	1.11 x 10^{-5}	2.05
7	-1.04	1050	9.17 x 10^{-6}	2.22
8	-1.05	1050	6.99 x 10^{-6}	2.09
9	-1.06	1050	7.87 x 10^{-6}	1.6
10	-1.1	1050	7.4 x 10^{-6}	1.1
15	-1.08	1000	1.54 x 10^{-5}	-0.56
20	-1.11	1000	1.79 x 10^{-5}	-1.07
40	-1.17	1060	1.4 x 10^{-3}	-1.2
50	-1.16	1190	1 x 10^{-3}	-1.2

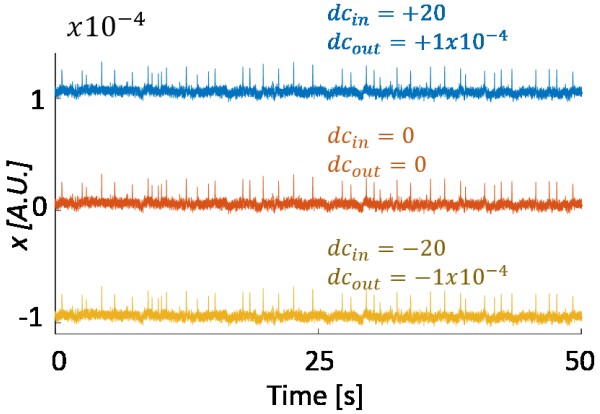

Figure 7. Different dc levels of the input signal change the stability point of the particle, and thus the dc level of the output signal. Input and output dc levels of the three cases are indicated for each plot. All output signals have identical SNR values of 1.1 dB.

2.4 Conventional pre-emphasis methods

To assess the detection performance of the proposed SR-based pre-emphasis method, we performed a comparison against the conventional methods of (i) band-pass filtering, (ii) TEO, and (iii) wavelet transform. Below we describe the implementation details of those methods.

Following the literature [6]; in band-pass filtering, the signal is filtered by a Kaiser-window FIR-filter with high-pass and low-pass cutoff frequencies of 300 Hz and 6 kHz.

Teager Energy Operator (TEO) emphasizes local peaks in both amplitude and frequency [43], thereby making it sensitive to spikes in a neural recording. The discrete-time TEO is given as:

$$\psi(x[n]) = x^2[n] - x[n+1] \cdot x[n-1]. \quad (7)$$

TEO suffers from degraded detection performance in low SNR and/or high noise peak scenarios [7, 41]. To smooth TEO output, following the literature [7], we use the Hamming-window FIR filter of length 5 with the following coefficients:

$$w(n) = [0.08\ 0.54\ 1\ 0.54\ 0.08]. \quad (8)$$

Discrete wavelet transform (DWT) is implemented with different mother wavelets with *sym4* being the most pronounced mother wavelet for pre-emphasizing in the literature [8, 44]. Accordingly, *sym4* is used as mother wavelet in this paper.

2.5 Thresholding for spike detection

Spikes in the pre-emphasized signals are determined via thresholding. Threshold levels giving the minimum false negative (FN) and false positive (FP) values are used. We use FN and FP values; and true-detection and false-alarm rates as performance assessment and comparison metrics.

True-detection rate (TDR) is defined as the ratio between number of spikes correctly detected (true positive, TP) and the total number of spikes in recording. False alarm rate (FAR) is defined as the number of falsely detected spikes (FP) per second.

$$TPR\ (\%) = \frac{TP}{TP + FN} * 100$$
$$FAR = \frac{FP}{recording\ time\ (s)}. \quad (9)$$

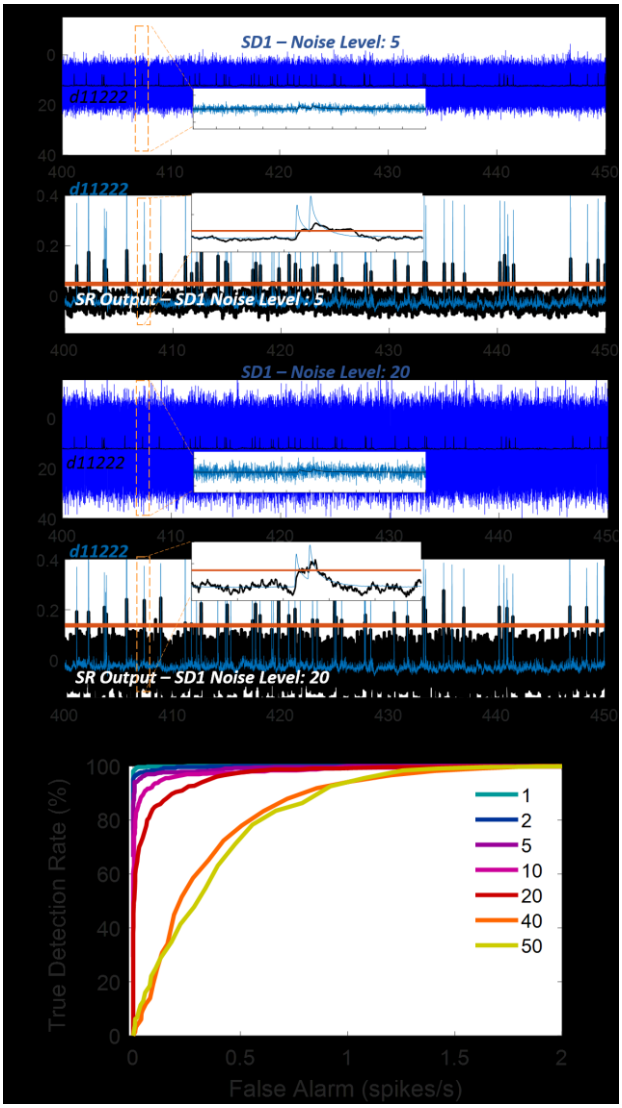

Figure 8. The response of the SR-based pre-emphasis method to SD1. 50 s portions of the input, the output, and the intracellular recording for the noise level of 5 and 20 are presented in (a) and (b). In the upper plots of each section, the original amplitudes of the noise-added input signal and the d11222 are shown. In the lower plots, the amplitudes of the SR output and the d11222 are normalized for visualization purposes. The close-up views (insets) show the noisy input and demonstrate the spike enhancement and noise suppression for one of the spikes. The threshold levels are shown as the horizontal red lines. (c) For different noise levels, the ROC curves are plotted. The area under the curves (AUCs) range from 199.2 (Noise Level 1) to 144.6 (Noise Level 50).

2.6 Receiver operating characteristic (ROC)

Receiver operating characteristic (ROC) curves of pre-emphasis methods are extracted by changing the detection threshold from 0.1σ to 8σ, where σ is the standard deviation of the noise segment. Based on TPR and FAR values for each level of detection threshold, ROC curves are plotted and then area under curve (AUC) is calculated.

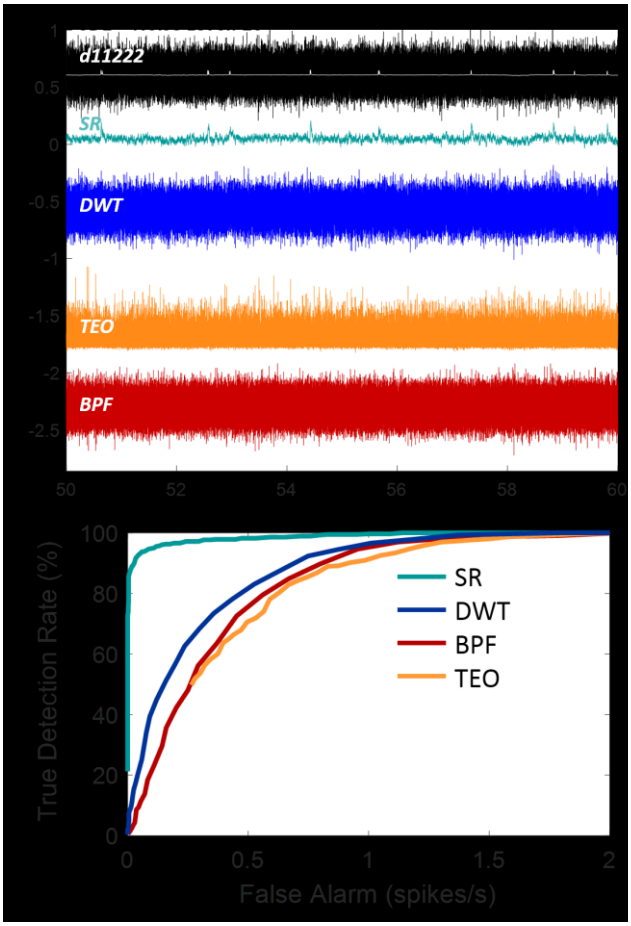

Figure 9. Comparison of the SR-based pre-emphasis method output to SD1 with the commonly-used methods. (a) 10 s portions of the outputs of the SR-based, DWT, TEO, and BPF pre-emphasis methods to the SD1 with noise level: 10 are shown. Amplitudes of the SD1 and the output waveforms are normalized. A scaled version of the d11222 is also shown to indicate the spike locations. (b) The ROCs for all methods.

3. Results

After optimizing the SR-based pre-emphasis method for different background noise intensities, we obtained the TPR and FAR for the SD1. For SD1 with noise levels of 5 (SNR_{in} =-0.96 dB) and 20 (SNR_{in} =-1.11 dB); the original intracellular recording, the noise-added input signal, the SR-based pre-emphasized output, and the threshold level are presented for a 50 s portion of the signals in Figure 8(a, b). To demonstrate the enhancement of the spikes, we highlight one of the spikes. For these two SD1 signals, SNR improvements calculated as the SNR differences between the SR output and the noisy input signal ($\Delta SNR=SNR_{out}-SNR_{in}$) are 3.89 dB and 0.4 dB. The receiver operating characteristic curves (ROC) for a range of noise levels between 1 (SNR_{in}=0.3 dB) and 50 (SNR_{in}=-1.16 dB) are presented in Figure 8(c). For noise levels <10 (SNR_{in}>-1.1 dB) the AUC of the curves are greater than 98% of the maximum area. The outputs of the proposed SR-based pre-emphasis method and those of BPF, TEO, and wavelet

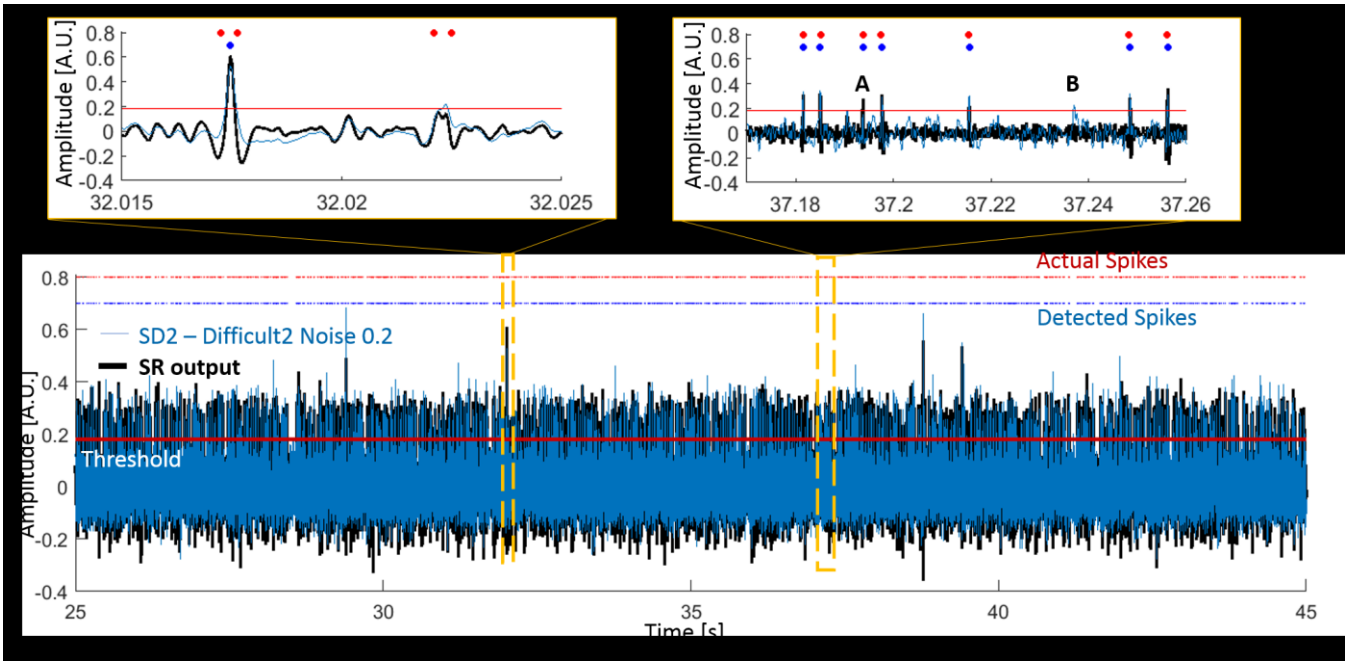

Figure 10. A 20 s section of the SR-based pre-emphasis method output for the SD2 dataset with the least spike detection accuracy, Difficult2 Noise 0.2. The close-up view on the left shows three of the 24 total missed spikes in this dataset. In general, overlapping spikes are missed. The close-up view on the right demonstrates the SR-output preventing a false negative (A) and a false positive (B).

transform for a 10 s portion of the SD1 with a noise level of 10 (SNR_{in}=-1.1 dB) are presented in Figure 9(a). The ROCs are presented in Figure 9(b). The SR-based pre-emphasis method AUC is 97% of the maximum area, whereas the other methods achieve AUC<77%.

The proposed method improves the threshold-detection of the recordings in the SD2. In Figure 10; the input, SR output, threshold level, actual and detected spike locations are presented for a 20 s portion of the SD2 recording with the least detection accuracy, namely *Difficult2 - Noise 0.2*. Majority of the 24 missed spikes in this recording are overlapping, three of which are highlighted in Figure 10; where examples of spike enhancement (A) and noise suppression (B) are also highlighted. For the complete SD2 datasets, we summarize the detection performance of the SR-based pre-emphasis method in Table 2. For comparison, we also present the spike detection accuracies of the state-of-the-art methods using the same datasets. Notably, compared to the best performing method in [14], where Bayes optimal template-matching (BOTM) and subtractive interference cancellation (SIC) are used, our

Table 2. Detection performance of the proposed method and the other state-of-the-art using the synthetic-dataset-2 in [6]

		# of Spikes	*This Work* Stochastic-Resonance				[14] Wave_clus, BOTM, SIC		[15] PBOTM		[33] Two side thresholding		[6] BPF		[35] MRTDE	
			#FN	*#FP*	*Se (%)*	*Pp (%)*	*# FN + FP*	*Se (%)*	*# FN + FP*	*Se (%)*	*#FN*	*#FP*	*#FN*	*# FP*	*Se (%)*	*Pp (%)*
Easy1	0.05	3514	0	0	100	100	11	99.7	68	98.1	17	9	17	711	93.75	100
	0.1	3522	2	0	99.95	100	4	99.9	58	98.4	26	32	2	57	93.28	100
	0.15	3477	5	3	99.86	99.92	8	99.8	63	98.2	61	114	145	14	95.50	100
	0.2	3474	4	4	99.89	99.89	9	99.7	84	97.6	170	212	714	10	95.54	99.07
Easy2	0.05	3410	0	0	100	100	2	99.9	58	98.3	34	5	0	0	92.86	100
	0.1	3520	0	0	100	100	6	99.8	47	98.7	27	2	0	2	93.60	100
	0.15	3411	0	1	100	99.97	4	99.9	52	98.5	55	12	10	1	93.33	98.00
	0.2	3526	5	4	99.86	99.89	6	99.8	78	97.8	259	157	376	5	90.60	99.07
Diff1	0.05	3383	0	0	100	100	2	99.9	58	98.3	30	0	1	63	93.07	100
	0.1	3448	0	0	100	100	18	99.5	57	98.3	34	4	0	10	96.08	100
	0.15	3472	1	0	99.97	100	9	99.7	61	98.2	68	21	8	6	95.83	100
	0.2	3414	5	4	99.85	99.88	20	99.4	92	97.3	175	169	184	2	96.15	100
Diff2	0.05	3364	0	0	100	100	8	99.8	53	98.4	31	2	0	1	94.44	100
	0.1	3462	0	0	100	100	5	99.9	38	98.9	21	2	0	5	95.50	100
	0.15	3440	4	2	99.88	99.94	8	99.8	61	98.2	60	33	3	4	92.38	100
	0.2	3493	24	1	99.31	99.97	36	99.0	91	97.4	302	162	262	2	91.00	92.86

BOTM = Bayes optimal template matching, SIC = Subtractive interference cancellation, PBOTM = Preselection Bayes optimal template matching, BPF = Band-pass filtering, MRTDE = Multiresolution time-dependent entropy

Table 3. Correlation coefficient values of spikes of the SD2 dataset.

		Easy1			Easy2			Difficult1			Difficult2		
		N1	N2	N3	N1	N2	N3	N1	N2	N3	N1	N2	N3
Noise 005	N1	1	0.3175	0.4163	1	0.8071	0.8788	1	0.8007	0.9166	1	0.9739	0.82
	N2	0.3175	1	0.1621	0.8071	1	0.8473	0.8007	1	0.9053	0.9739	1	0.81
	N3	0.4163	0.1621	1	0.8788	0.8473	1	0.9166	0.9053	1	0.82	0.81	1
Noise 01	N1	1	0.3032	0.4069	1	0.8029	0.8752	1	0.8015	0.9212	1	0.9735	0.8235
	N2	0.3032	1	0.163	0.8029	1	0.8399	0.8015	1	0.9039	0.9735	1	0.8107
	N3	0.4069	0.163	1	0.8752	0.8399	1	0.9212	0.9039	1	0.8235	0.8107	1
Noise 015	N1	1	0.3102	0.398	1	0.8033	0.8771	1	0.8061	0.9257	1	0.9722	0.8262
	N2	0.3102	1	0.1669	0.8033	1	0.8494	0.8061	1	0.9093	0.9722	1	0.8082
	N3	0.398	0.1669	1	0.8771	0.8494	1	0.9257	0.9093	1	0.8262	0.8082	1
Noise 02	N1	1	0.3007	0.4197	1	0.8039	0.869	1	0.8005	0.9226	1	0.9747	0.8176
	N2	0.3007	1	0.1452	0.8039	1	0.8353	0.8005	1	0.9017	0.9747	1	0.8102
	N3	0.4197	0.1452	1	0.869	0.8353	1	0.9226	0.9017	1	0.8176	0.8102	1

results exhibit better detection performance for fifteen of the datasets, and comparable performance for the remaining dataset, namely *Easy2 – Noise 0.2*.

In this study, we limit our focus to spike detection only. On the other hand, in neurophysiology research and neural monitoring applications, it is important to accurately sort the detected spikes. Spike sorting performance is affected by waveform shape similarities within spikes originated by the same neuron and dissimilarities among spikes from different neurons [45]. To investigate if the proposed pre-emphasis method could potentially enable accurate sorting of the detected spikes, we performed a similarity/dissimilarity analysis on the pre-emphasized spikes of SD2. Specifically, we performed a correlation analysis quantified by Pearson's correlation coefficient, r, on the spike waveforms of the SR-based pre-emphasis outputs. Our analysis consists of the following three steps:

- We performed a baseline correlation analysis on spikes of the SD2 before pre-emphasis. Here, for a given recording (e.g., Easy1_005), we obtained a template of each spike type (neuron 1, neuron 2, or neuron 3) by ensemble averaging all spikes under the same type. Then, we performed cross- and auto-correlation on the templates of spikes (Table 3).

- We performed a correlation analysis on spikes pre-emphasized by the proposed method. Here, for a given SR-based pre-emphasis output recording, we obtained a template

Table 4. Correlation coefficient values of spikes of the SR-based pre-emphasized SD2 dataset (Template vs. Individual spikes).

		Easy1			Easy2			Difficult1			Difficult2		
		N1	N2	N3	N1	N2	N3	N1	N2	N3	N1	N2	N3
Noise005	N1	0.714 (0.116)	0.617 (0.072)	0.67 (0.06)	0.935 (0.081)	0.692 (0.102)	0.766 (0.092)	0.86 (0.111)	0.875 (0.095)	0.907 (0.076)	0.932 (0.095)	0.899 (0.085)	0.818 (0.107)
	N2	0.168 (0.048)	0.869 (0.075)	0.141 (0.044)	0.85 (0.07)	0.924 (0.099)	0.747 (0.083)	0.794 (0.089)	0.876 (0.013)	0.878 (0.07)	0.93 (0.092)	0.942 (0.082)	0.821 (0.104)
	N3	0.071 (0.072)	0.231 (0.076)	0.873 (0.076)	0.887 (0.079)	0.777 (0.107)	0.889 (0.101)	0.75 (0.099)	0.868 (0.096)	0.915 (0.074)	0.699 (0.095)	0.674 (0.093)	0.917 (0.104)
Noise01	N1	0.781 (0.124)	0.515 (0.085)	0.569 (0.047)	0.916 (0.08)	0.671 (0.117)	0.745 (0.115)	0.836 (0.107)	0.856 (0.088)	0.888 (0.075)	0.912 (0.085)	0.882 (0.087)	0.799 (0.107)
	N2	0.189 (0.069)	0.889 (0.084)	0.15 (0.05)	0.83 (0.072)	0.897 (0.103)	0.718 (0.098)	0.73 (0.089)	0.856 (0.092)	0.862 (0.066)	0.911 (0.082)	0.926 (0.082)	0.802 (0.103)
	N3	0.142 (0.124)	0.22 (0.118)	0.927 (0.057)	0.861 (0.085)	0.746 (0.124)	0.862 (0.113)	0.736 (0.108)	0.856 (0.094)	0.898 (0.073)	0.688 (0.094)	0.666 (0.099)	0.895 (0.1)
Noise015	N1	0.752 (0.124)	0.496 (0.103)	0.552 (0.065)	0.886 (0.091)	0.642 (0.124)	0.718 (0.118)	0.803 (0.111)	0.819 (0.091)	0.861 (0.078)	0.864 (0.102)	0.845 (0.099)	0.763 (0.117)
	N2	0.192 (0.086)	0.858 (0.098)	0.155 (0.081)	0.805 (0.079)	0.865 (0.092)	0.701 (0.097)	0.693 (0.102)	0.819 (0.095)	0.832 (0.072)	0.865 (0.098)	0.891 (0.09)	0.763 (0.11)
	N3	0.131 (0.156)	0.208 (0.151)	0.901 (0.081)	0.834 (0.095)	0.725 (0.122)	0.829 (0.109)	0.708 (0.125)	0.817 (0.105)	0.868 (0.082)	0.657 (0.124)	0.643 (0.12)	0.856 (0.102)
Noise02	N1	0.709 (0.126)	0.48 (0.114)	0.561 (0.07)	0.707 (0.104)	0.478 (0.113)	0.482 (0.137)	0.758 (0.113)	0.772 (0.102)	0.83 (0.079)	0.825 (0.109)	0.817 (0.11)	0.718 (0.13)
	N2	0.181 (0.115)	0.828 (0.106)	0.145 (0.126)	0.751 (0.09)	0.726 (0.096)	0.5181 (0.123)	0.666 (0.107)	0.775 (0.103)	0.802 (0.075)	0.826 (0.103)	0.853 (0.098)	0.723 (0.121)
	N3	0.1346 (0.1943)	0.198 (0.172)	0.851 (0.168)	0.715 (0.104)	0.563 (0.118)	0.574 (0.131)	0.672 (0.139)	0.767 (0.125)	0.836 (0.092)	0.634 (0.14)	0.625 (0.135)	0.808 (0.118)

Table 5. Correlation coefficient changes with respect to the baseline.

		Easy1			Easy2			Difficult1			Difficult2		
		N1	N2	N3	N1	N2	N3	N1	N2	N3	N1	N2	N3
Noise 005	N1	-0.286	0.3	0.253	-0.065	-0.115	-0.113	-0.141	0.075	-0.010	-0.068	-0.075	-0.002
	N2	-0.145	-0.131	-0.021	0.042	-0.077	-0.101	-0.006	-0.124	-0.027	-0.044	-0.058	0.011
	N3	-0.346	0.069	-0.127	0.008	-0.066	-0.111	-0.166	-0.037	-0.085	-0.121	-0.136	-0.083
Noise 01	N1	-0.219	0.211	0.163	-0.084	-0.132	-0.131	-0.164	0.055	-0.032	-0.088	-0.091	-0.024
	N2	-0.114	-0.11	-0.02	0.027	-0.104	-0.122	-0.072	-0.144	-0.042	-0.063	-0.074	-0.008
	N3	-0.27	0.057	-0.073	-0.014	-0.094	-0.138	-0.185	-0.048	-0.102	-0.135	-0.145	-0.105
Noise 015	N1	-0.248	0.186	0.154	-0.114	-0.161	-0.159	-0.197	0.013	-0.064	-0.136	-0.127	-0.063
	N2	-0.118	-0.142	-0.012	0.001	-0.135	-0.149	-0.114	-0.181	-0.077	-0.108	-0.109	-0.046
	N3	-0.267	0.041	-0.099	-0.043	-0.124	-0.171	-0.218	-0.093	-0.132	-0.169	-0.165	-0.144
Noise 02	N1	-0.291	0.18	0.141	-0.293	-0.326	-0.387	-0.242	-0.028	-0.093	-0.175	-0.158	-0.1
	N2	-0.12	-0.172	0.001	-0.053	-0.274	-0.317	0.134	-0.226	-0.1	-0.149	-0.147	-0.087
	N3	-0.285	0.053	-0.149	-0.154	-0.272	-0.427	-0.251	-0.135	-0.164	-0.184	-0.186	-0.192

of each spike type (neuron 1, neuron 2, or neuron 3) by ensemble averaging all spikes under the same type. Then, we performed cross- and auto-correlation between template of a spike type and individual spikes of the other two spike types. We present the mean and standard deviations of the correlation results (Table 4).

- We performed an analysis of how correlation coefficients obtained in step 2 change from the baseline values obtained in step 1 (Table 5). Here, a negative change in cross-correlation coefficients corresponds to a reduced similarity between different spike types, and thus is desired. We use red colour to highlight those cases.

4. Discussion

The large damping of the system and the existence of a stability point in the well collectively limit the movement of the particle when the tilt direction and magnitude rapidly changes with noise. However, a spike added with noise causes the well to tilt persistently in one direction, thereby causing larger movements of the particle resulting in SNR improvement for different noise levels as presented in Table 1. In general, the SNR improvement, ΔSNR, decreases with the added noise level and reaches ~0 dB for noise levels >~20 (Figure 11). Notably, the trend of the ΔSNR decrease is disrupted for noise levels between 6 and 10 with a local maximum occurring at a noise level of 7 (Figure 11 - inset). This behaviour can be explained by the contribution of additive noise on spike enhancement dynamics. During a spike event, the additive noise serves as a facilitator increasing the likelihood of the particle move further away from the stable point, thereby strengthening the spike. This enhancement becomes more prominent for a range of noise levels, and thus resulting in a curve similar to the characteristic bell curve of stochastic resonance, where SNR improvement is greater for a particular range of non-zero noise levels [32, 37].

The comparison of our pre-emphasis method against state-of-the-art pre-emphasis methods (i.e., BPF, TEO, and wavelet transform) reveal that, our approach offers greater SNR improvement even for high background noise levels. Accordingly, we anticipate that our pre-emphasis method enabling detection of activities from distant neurons.

In terms of spike detection performance, our method of SR-based pre-emphasising followed by thresholding offers comparable performance to the state-of-the-art template-based spike detection method in [6]. Unlike the template-based methods however, our approach potentially does not suffer from poor detection performance of spikes from low-activity neurons.

The proposed method can contribute to the field of neural monitoring by potentially increasing the number of spikes that can be monitored from a recording captured by a single electrode. Despite a theoretical number of ~1000 neurons from which an electrode can record from; presently, the number of sortable spikes in an extracellular recording is

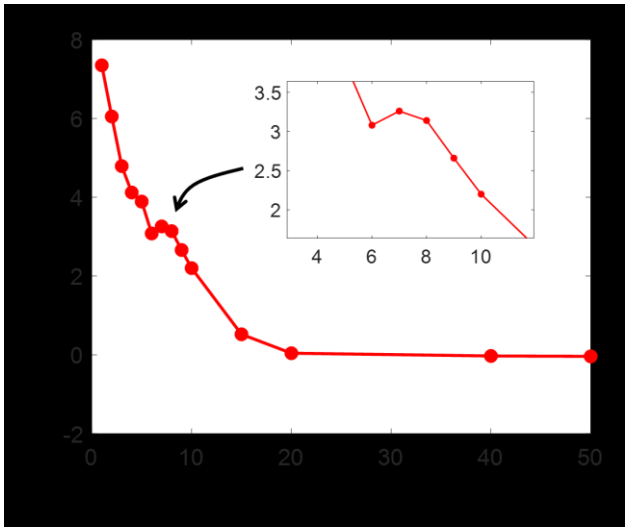

Figure 11. The SNR improvements of the SR-based pre-emphasis on SD1 with different noise intensities.

limited to 5-10 [17-18]. Importantly, there are two major reasons limiting the number.

First, the state-of-the-art spike detection algorithms that perform significantly better than other spike detection methods such as [6] follow template-based spike detection approaches, which causes them to perform poorly in detecting the spikes of sparsely firing neurons [16]. The first advantage of our approach is that, it does not require waveform templates for spike detection. Therefore, we anticipate that our method would accurately detect spikes regardless of the activity levels of the originating neurons.

Second, spikes from distant neurons have amplitudes smaller than the threshold, causing them to go unnoticed even at the spike detection stage. Based on our results from SD1, the proposed method offers better SNR improvement compared to standard pre-emphasizing methods of BPF, TEO, and wavelet transform. Therefore, the second advantage of the proposed approach is that, it could potentially detect spikes created inside a larger radius than existing methods.

Based on our correlation analysis of spikes, the proposed SR-based pre-emphasis methods improves the dissimilarity between spikes of different neurons in 74 of the 96 different comparison combinations with an average improvement (decrease in correlation coefficients) of 0.12±0.08. In the remaining 22 combinations, the average deterioration in dissimilarities is small (0.099±0.088). The results indicate that, in most of the datasets, spike sorting on the spikes pre-emphasized using the proposed method could potentially lead to higher classification accuracy compared to the original spikes in the datasets. The pre-emphasized spike outputs can be sorted using the state-of-the-art spike sorting algorithms such as superparamagnetic clustering [6], MountainSort [46], or KiloSort [47].

The noise suppression mechanism of the proposed method and the enhancement of the features with persistent changes in one direction bears a resemblance to a moving window averaging (MWA) filter; where the smoothed version of the output emphasizes the portions of the signal with persistent change (e.g., a noisy spike) while suppressing the noise-only sections. However, there are clear differences between the two approaches, which we demonstrate on SD1, where spikes are from the same neuron (Figure 12). First, an MWA filter generates spikes advancing the actual spike onset. As the window length (WL) is increased, the time difference between the onsets of the actual spike and the spike at the output increases, which impairs the time resolution of spike events at the output. On the other hand, the SR-based pre-emphasis method follows the abrupt and persistent changes quickly, thereby potentially enabling high detection specificity for overlapping spikes. Second; compared to an MWA filter with a short WL that can offer better time resolution (e.g., WL: 5 ms in Figure 12); the SR-based method offers better noise suppression, thereby resulting in higher SNR (Figure 12).

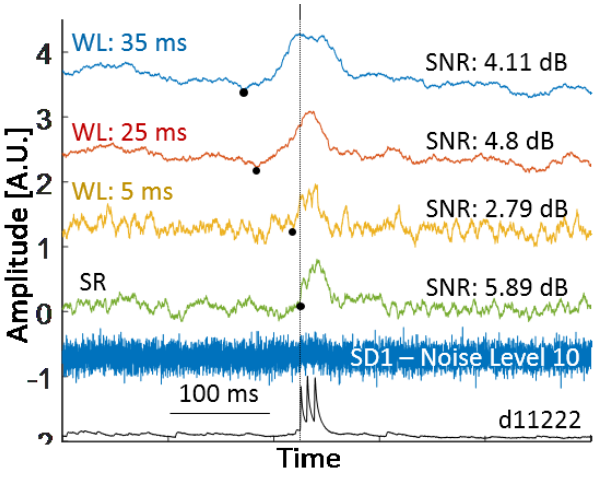

Figure 12. Comparison of the SR-based pre-emphasis method with a moving window averaging (MWA) filter. The outputs of the SR and MWA with different window lengths (WL) are shown for a 500 ms segment of the SD1 – Noise Level 10. The vertical line shows the spike onset and the black dots show the spike onsets at the outputs.

There are three major limitations of the proposed pre-emphasis and spike detection method. First, there is an upper bound of SNR_{in} for which a meaningful ΔSNR increase is observed. Accordingly, the spike detection performance is limited for high input noise levels. In an actual recording scenario, these results indicate that, to a first order approximation, there is a maximum distance within which the spikes can be enhanced. Second, spike detection performance degrades for some overlapping spikes. It should be noted that, in this study, where we present the analysis of a SR-based pre-emphasis method of neural spikes for the first time, we use a monostable well potential. Further analysis on different well potentials could be investigated to address these limitations. Third, in the proposed spike detection method, threshold needs to be adjusted to maximize the sensitivity and positive predictivity. Likewise, to maximize the detection performance, the parameters a and h need to be optimized for different noise levels of the neural recording (SNR_{in}). These characteristics might suggest that, spike detection from a single-channel extracellular recording can be optimized by using multiple SR-based detectors, each tuned to maximize the detection of spikes for a range of spike amplitudes.

Additionally, there are several limitations of this study related to the datasets used. First, we use an intracellular-recording-based synthetic dataset, SD1, to demonstrate the attributes of the dynamics of the system at the desired granularity by precisely controlling the background noise. However, the shape of an intracellular spike in SD1 does not accurately reflect the spikes that are seen in an extracellular recording, such as the ones in the synthetic dataset SD2. Furthermore, we only use a Gaussian white noise to model the background noise in SD1. Accordingly, the SNR improvements and the ROC AUCs obtained for different

background noise levels could be potentially different from an actual extracellular recording with similar background noise intensities. It should be noted that, different noise types (i.e., white or colored) could result in different levels of improvements in SNR and spike detection performances [27, 49, 50]. The effects of different noise types on the proposed method could be investigated to unveil these differences. Notably, the background noise of an extracellular recording consists of different noise types including white and colored noise originated from different sources related to the measurement setup and environment (e.g., electrode impedance, electromyogram) [51]. Therefore, such an investigation could provide insights on the design of the measurement setup.

The results of this study could find applications across different neuroscience studies, where noise is investigated in the context of physiological responses of the brain. Specifically, our approach of SNR-based optimal system parameter identification for a given noise level can be expanded to optimizing the neurostimulation noise level that maximizes the physiological firing responses of neurons [48].

5. Conclusion and future work

This paper presents a pre-emphasis method facilitating stochastic resonance for spike detection in neural recordings. We demonstrated quantitatively that, the dynamics of a Brownian particle in a damped monostable-well can be used to improve spike detectability by suppressing noise while enhancing spikes. The presence of a stability point and the large damping of the particle suppresses the noise-only sections of the recordings. Specifically, we show that, the spike enhancement of the additive noise is more noticeable for a range of noise levels. Our results on a public synthetic dataset demonstrate the spike enhancement and noise suppression, as well as a spike detection performance surpassing the state-of-the-art.

In future works, towards reaching an error-free spike detection performance, we will investigate multiple SR-based pre-emphasis and spike-detector systems operating in parallel. As a first step, we will expand our results in this study on synthetic extracellular datasets enabling precise control of the intensity of accurately modelled background noise. These datasets will enable us to investigate the correlations between background noise level/spike amplitude in a given extracellular dataset and the variables of the well/solver, which can then be used to identify the architecture and parameters of a multiple spike detector system.

6. Acknowledgments

This work was supported by the U.S. National Science Foundation under Grant #1916160.

References

[1] C. Keysers, E. Kohler, M.A. Umiltà et al. 2003 “Audiovisual mirror neurons and action recognition.” *Exp Brain Res* **153** 628–636

[2] D. Khodagholy, J. Gelinas, T. Thesen et al. 2015 “NeuroGrid: recording action potentials from the surface of the brain.” *Nat Neurosci* **18** 310–315

[3] E. Brown, R. Kass, P. Mitra 2004 “Multiple neural spike train data analysis: state-of-the-art and future challenges.” *Nat Neurosci* **7** 456–461

[4] J.K. Kleen, R.C. Scott, G. L. Holmes, P. P. Lenck-Santini 2010 “Hippocampal interictal spikes disrupt cognition in rats.” *Ann Neurol.* **67** 250-257 (doi:10.1002/ana.21896)

[5] S. Spencer 2002 “Neural Networks in Human Epilepsy: Evidence of and Implications for Treatment.” *Epilepsia* **43** 219-227 (doi:10.1046/j.1528-1157.2002.26901.x)

[6] R. Quian Quiroga, Z. Nadasdy, Y. Ben-Shaul 2004 “Unsupervised spike detection and sorting with wavelets and superparamagnetic clustering.” *Neural Comput* **16** 1661-1687

[7] H. Semmaoui, J. Drolet, A. Lakhssassi and M. Sawan 2012 "Setting Adaptive Spike Detection Threshold for Smoothed TEO Based on Robust Statistics Theory," *IEEE Transactions on Biomedical Engineering* **59** 474-482

[8] V. Shalchyan, W. Jensen and D. Farina 2012 "Spike Detection and Clustering With Unsupervised Wavelet Optimization in Extracellular Neural Recordings," *IEEE Transactions on Biomedical Engineering* **59** 2576-2585

[9] K. Sunghan, M. James 2007 “Automatic spike detection based on adaptive template matching for extracellular neural recordings.” *J Neurosci Methods* **165** 165–174

[10] S. Shahid, J. Walker and L. S. Smith 2010 "A New Spike Detection Algorithm for Extracellular Neural Recordings," *IEEE Transactions on Biomedical Engineering* **57** 853-866

[11] H. S. Bokil, B. Pesaran, R. A. Andersen and P. P. Mitra 2006 "A Method for Detection and Classification of Events in Neural Activity," *IEEE Transactions on Biomedical Engineering* **53** 1678-1687

[12] X. Liu, X. Yang, N. Zheng 2012 "Automatic extracellular spike detection with piecewise optimal morphological filter." *Neurocomputing* **79** 132 – 139

[13] K. J. Laboy-Juárez, S. Ahn, D.E. Feldman 2019 “A normalized template matching method for improving spike detection in extracellular voltage recordings.” *Sci Rep.* **9**

[14] F. Franke, R. Quian Quiroga, A. Hierlemann et al. 2015 “Bayes optimal template matching for spike sorting – combining fisher discriminant analysis with optimal filtering.” *J Comput Neurosci* **38** 439–459

[15] H. Xu, Y. Han, X. Han et. al. 2019 “Unsupervised and real-time spike sorting chip for neural signal processing in hippocampal prosthesis.” *Journal of Neuroscience Methods* **311** 111–121

[16] H.G. Rey, C. Pedreira, R. Quian Quiroga 2015 “Past, present and future of spike sorting techniques.” *Brain Res Bull* **119** 106–117 (doi:10.1016/j.brainresbull.2015.04.007)

[17] P. Carlos, J. Martinez, M. J. Ison, R. Quian Quiroga 2012 "How many neurons can we see with current spike sorting algorithms?" *Journal of neuroscience methods* **211** 58-65

[18] D. A. Henze, Z. Borhegyi, J. Csicsvari, A. Mamiya, K.D. Harris, G. Buzsáki 2000 “Intracellular Features Predicted by

Extracellular Recordings in the Hippocampus In Vivo," *Journal of Neurophysiology* **84** 390-400

[19] D. Dai, Q. He 2012 "Multiscale noise tuning stochastic resonance enhances weak signal detection in a circuitry system," *Measurement Science and Technology* **23**

[20] H. Zhang, W. Xiong, S. Zhang, et al. 2016 "Nonstationary weak signal detection based on normalization stochastic resonance with varying parameters," *Sādhanā* **41** 621–632

[21] Z. Zhang, J. Ma. 2019 "Adaptive parameter-tuning stochastic resonance based on SVD and its application in weak IF digital signal enhancement," *EURASIP J. Adv. Signal Process* **24**

[22] J. Liu, Y. Leng, Z. Lai, S. Fan 2018 "Multi-Frequency Signal Detection Based on Frequency Exchange and Re-Scaling Stochastic Resonance and Its Application to Weak Fault Diagnosis," *Sensors* **18**

[23] R. Benzi, A. Sutera, A. Vulpiani 1981 "The mechanism of stochastic resonance," *J. Phys. A Math. Gen.* **14** 453–457

[24] F. Moss, M. W. Lawrence, G. S. Walter 2004 "Stochastic resonance and sensory information processing: a tutorial and review of application." *Clinical neurophysiology* **115** 267-281

[25] D. F. Russell, A. W. Lon, F. Moss 1999 "Use of behavioural stochastic resonance by paddle fish for feeding." *Nature* **402**

[26] F. Jaramillo, W. Kurt 1998 "Mechanoelectrical transduction assisted by Brownian motion: a role for noise in the auditory system." *Nature neuroscience* **1**

[27] Eisen, Erik S. and Hakan Töreyin 2019 "A Preliminary Analysis on Impact of Additive Flicker Noise on Detection Sensitivity of Neural Spikes." *2019 41st Annual International Conference of the IEEE Engineering in Medicine and Biology Society (EMBC)* 5164-5167

[28] Y. Liu, F. Wang, L. Liu, Y. Zhu 2019 "Secondary signal-induced large-parameter stochastic resonance for feature extraction of mechanical faults." *International Journal of Modern Physics B* **33**

[29] D. Huang, J. Yang, D. Zhou et. al. 2019 "Recovering an unknown signal completely submerged in strong noise by a new stochastic resonance method." *Communications in Nonlinear Science and Numerical Simulation* **66** 156–166

[30] D. Huang, J. Yang, J. Zhang, H. Liu 2018 "An improved adaptive stochastic resonance with general scale transformation to extract high-frequency characteristics in strong noise." *International Journal of Modern Physics B* **32**

[31] Z. Qiao, Y. Lei, N. Li 2019 "Applications of stochastic resonance to machinery fault detection: A review and tutorial." *Mechanical Systems and Signal Processing* **122** 502–536

[32] L. Gammaitoni, P. Hanggi, P. Jung, F. Marchesoni 1998 "Stochastic resonance" *Rev. Mod. Phys.* **70** 223-287

[33] D. A. Henze, K. D. Harris, Z. Borhegyi, J. Csicsvari, A. Mamiya, H. Hirase, A. Sirota, G. Buzsáki 2009 "Simultaneous intracellular and extracellular recordings from hippocampus region CA1 of anesthetized rats." CRCNS.org (http://dx.doi.org/10.6080/K02Z13FP)

[34] M. Moghaddasi, M. Aliyari Shoorehdeli, Z. Fatahi, A. Haghparast 2020 "Unsupervised automatic online spike sorting using reward-based online clustering." *Biomedical Signal Processing and Control* **56**

[35] X. Liu, H. Wan, Z. Shang, L. Shi 2015 "Automatic extracellular spike denoising using wavelet neighbor coefficients and level dependency." *Neurocomputing* **149** 1407-1414

[36] S. Farashi 2018 "Spike detection using a multiresolution entropy based method." *Biomedical Engineering / Biomedizinische Technik* **63** 361-376 (doi: https://doi.org/10.1515/bmt-2016-0182)

[37] B. McNamara, K, Wiesenfeld 1989 "Theory of stochastic resonance." *Phys. Rev. A* **39** 4854-4869

[38] A. S. Asdi, A. H. Tewfik 1995 "Detection of weak signals using adaptive stochastic resonance," *International Conference on Acoustics, Speech, and Signal Processing, Detroit, MI, USA* **2** 1332-1335

[39] S. Gibson, J. W. Judy and D. Markovic 2010 "Technology-Aware Algorithm Design for Neural Spike Detection, Feature Extraction, and Dimensionality Reduction," *IEEE Transactions on Neural Systems and Rehabilitation Engineering* **18** 469-478

[40] K. H. Kim and S. J. Kim 2000 "Neural spike sorting under nearly 0-dB signal-to-noise ratio using nonlinear energy operator and artificial neural-network classifier," *IEEE Transactions on Biomedical Engineering* **47** 1406-1411

[41] l. Obeid 2007 "Comparison of Spike Detectors based on Simultaneous Intracellular and Extracellular Recordings," *3rd International IEEE/EMBS Conference on Neural Engineering*, *Kohala Coast, HI* 410-413

[42] S. Shahid, J. Walker and L. S. Smith 2010 "A New Spike Detection Algorithm for Extracellular Neural Recordings," *IEEE Transactions on Biomedical Engineering* **57** 853-866

[43] J. H. Choi, H. K. Jung, T. Kim 2006 "A new action potential detector using the MTEO and its effects on spike sorting systems at low signal-to-noise ratios," *IEEE Transactions on Biomedical Engineering* **53** 738-746

[44] G. C. F. Lee, C. Libedinsky, C. Guan, R. So 2017 "Use of wavelet transform coefficients for spike detection for a Robust Intracortical Brain Machine Interface," *2017 8th International IEEE/EMBS Conference on Neural Engineering (NER)*, *Shanghai* 540-543

[45] C. R. Caro-Martín, , J. M. Delgado-García, A. Gruart, R. Sánchez-Campusano 2018 "Spike sorting based on shape, phase, and distribution features, and K-TOPS clustering with validity and error indices." *Scientific Reports*, **8** 1-28.

[46] J. E. Chung, F. Magland, A. H. Barnett, V. M. Tolosa, et. Al. 2017 "A fully automated approach to spike sorting." *Neuron* **95** 1381-1394

[47] M. Pachitariu, N. A. Steinmetz, S. N. Kadir, M. Carandini, K. D. Harris 2016 "Fast and accurate spike sorting of high-channel count probes with KiloSort." *Advances in neural information processing systems* 4448-4456

[48] N. Huidobro B. De la Torre-Valdovinos, A. Mendez et. al. 2018 "Optogenetic noise-photostimulation on the brain increases somatosensory spike firing responses," *Neuroscience Letters,* **664** 51-57

[49] R. Soma, D. Nozaki, S. Kwak,Y. Yamamoto 2003 "1/f Noise Outperforms White Noise in Sensitizing Baroreflex Function in the Human Brain," *Phys. Rev. Lett.,* **91** 1-4

[50] D. Nozaki, D. J. Mar, P. Grigg, and J. J. Collins 1999 "Effects of colored noise on stochastic resonance in sensory neurons." *Physical Review Letters* **82** 2402-2405

[51] P.G. Musial, S. N. Baker, G. L. Gerstein, E. A. King, and J. G. Keating 2002 "Signal-to-noise ratio improvement in multiple electrode recording." *Journal of Neuroscience Methods* **115** 29-43